A GPS Positioning Approach Exploiting GSM Velocity Estimates

Sven Peschke, Maik Bevermeier, and Reinhold Haeb-Umbach
Department of Communications Engineering, University of Paderborn, Germany
Email: {peschke, bevermeier, haeb}@nt.uni-paderborn.de

***Abstract*—A combination of GPS (Global Positioning System) and INS (Inertial Navigation System) is known to provide high precision and highly robust vehicle localization. Notably during times when the GPS signal has a poor quality, e.g. due to the lack of a sufficiently large number of visible satellites, the INS, which may consist of a gyroscope and an odometer, will lead to improved positioning accuracy. In this paper we show how velocity information obtained from GSM (Global System for Mobile Communications) signalling, rather than from a tachometer, can be used together with a gyroscope sensor to support localization in the presence of temporarily unavailable GPS data. We propose a sensor fusion system architecture and present simulation results that show the effectiveness of this approach.**

I. Introduction

Vehicle positioning based solely on GPS signals suffers from a lack of robustness as it heavily relies on the visibility of a sufficiently large number of satellites. As the visibility, however, may be impaired, for example in narrow street canyons or in tunnels, GPS has to be backed up by additional positioning sensors if critical applications are to be realized.

For example, in the German electronic toll collect system the vehicle's position is tracked by a combination of GPS, gyroscope, and odometer data, the latter being acquired through a connection to the vehicle's CAN (Controller Area Network) bus. In the so-called *onboard unit* (OBU) the sensor data are fused and information relevant for toll computation is transmitted to a central station via a GSM link.

In this paper we consider the use of velocity information estimated from the GSM signal characteristics as a replacement of the odometer readings. As a GSM terminal is present in an OBU anyway, this would come at no extra hardware costs while at the same time rendering the costly installation of a CAN bus interface for access to the odometer data unnecessary.

As explained in a former WPNC paper [1], velocity estimates via GSM can be obtained from the fast fading statistics of received downlink signals without establishing an active connection. With the approach taken there, it turned out that the mean and variance of the measurement error depend on the true velocity.

Note that the use of GSM signal strength measurements to determine the vehicle's position [2] results in rather inaccurate estimates and will therefore not further considered here.

In this paper we show how a GSM based velocity estimator can be utilized in a positioning system and determine the achievable positioning accuracy by means of simulations. The paper is organized as follows: In the next section we explain the generation of artificial GPS, gyroscope, and GSM data in our simulation system. We then describe how the various sensor data, including GSM based velocity estimates, are processed and fused. In section IV we present experimental results before giving concluding remarks in section V.

II. Measurement Data Generation

Figure II gives an overview of the generation of the artificial measurement data, thus simulating a GPS, gyroscope, and GSM device. First, a random vehicle trajectory is generated which serves as the ground truth for the vehicle's position and velocity. From this, artificial GPS and gyroscope measurements are generated according to a measurement model which captures the imperfections of the corresponding devices. The ground truth forward velocity s is input to the GSM channel simulator as it affects the Doppler spectrum of the fading processes. The received GSM downlink signal is generated from which velocity estimates are to be obtained. In the following we are giving a detailed description of the simulation system.

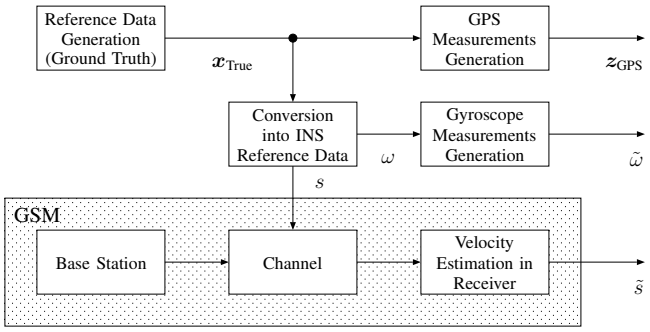

Fig. 1. Generation of measurement data

A. Generation of Ground Truth Values

First, artificial reference trajectories are generated, whose characteristics match the second order statistics of data gathered by real test drives. For every sampling time k, where k counts multiples of the sampling interval T_{Gyro} of the

gyroscope, the ground truth values of the vehicle's state

$$\boldsymbol{x}_{\text{True}}(k) = \begin{pmatrix} x(k{\cdot}T_{\text{Gyro}}) \\ y(k{\cdot}T_{\text{Gyro}}) \\ v_x(k{\cdot}T_{\text{Gyro}}) \\ v_y(k{\cdot}T_{\text{Gyro}}) \end{pmatrix} \tag{1}$$

are generated according to a state model described further below. The state vector $\boldsymbol{x}_{\text{True}}(k)$ contains the vehicle's current position $(x(k{\cdot}T_{\text{Gyro}}), y(k{\cdot}T_{\text{Gyro}}))$ and velocity components $(v_x(k{\cdot}T_{\text{Gyro}}), v_y(k{\cdot}T_{\text{Gyro}}))$, both in 2D-Cartesian coordinates. The sampling period $T_{\text{Gyro}} = \frac{24}{1625}$ [s] was chosen in relation to the sampling time T_{GSM} of the GSM based velocity estimator, as will be explained later on.

Assuming a dynamical model of type "constant acceleration" [3], the state equation is given by

$$\boldsymbol{x}_{\text{True}}(k+1) = \boldsymbol{A}_{\text{True}}\boldsymbol{x}_{\text{True}}(k) + \boldsymbol{B}_{\text{True}}\boldsymbol{w}_{\text{True}}(k). \tag{2}$$

with the state transition matrix

$$\boldsymbol{A}_{\text{True}} = \begin{pmatrix} 1 & 0 & T_{\text{Gyro}} & 0 \\ 0 & 1 & 0 & T_{\text{Gyro}} \\ 0 & 0 & 1 & 0 \\ 0 & 0 & 0 & 1 \end{pmatrix}. \tag{3}$$

The matrix

$$\boldsymbol{B}_{\text{True}} = \begin{pmatrix} \frac{T_{\text{Gyro}}^2}{2} & 0 \\ 0 & \frac{T_{\text{Gyro}}^2}{2} \\ T_{\text{Gyro}} & 0 \\ 0 & T_{\text{Gyro}} \end{pmatrix} \tag{4}$$

maps the white system noise $\boldsymbol{w}_{\text{True}}(k)$ to the state vector according to Newton's motion laws.

The system noise $\boldsymbol{w}_{\text{True}}(k) \sim \mathcal{N}(\boldsymbol{0}, 46.3 \cdot \boldsymbol{I}_2)$ is Gaussian with mean $\boldsymbol{0}$ and covariance $46.3 \cdot \boldsymbol{I}_2$, where $\boldsymbol{I}_n$ denotes a diagonal matrix of size $n{\times}n$. These values were obtained from an analysis of real field data of a test drive where the position was measured in [m] and the velocity was measured in $[\frac{\text{m}}{\text{s}}]$.

As a low cost GPS device delivers measurements at a much lower rate than the gyroscope rate $\frac{1}{T_{\text{Gyro}}}$ (in this paper we assume a typical GPS sampling interval of $T_{\text{GPS}} = 1$ [s]), we make a distinction in our notation between the vehicle state trajectory at rate $\frac{1}{T_{\text{Gyro}}}$ and $\frac{1}{T_{\text{GPS}}}$. To be specific,

$$\boldsymbol{x}'_{\text{True}}(m) = \begin{pmatrix} x(m{\cdot}T_{\text{GPS}}) \\ y(m{\cdot}T_{\text{GPS}}) \\ v_x(m{\cdot}T_{\text{GPS}}) \\ v_y(m{\cdot}T_{\text{GPS}}) \end{pmatrix}, \tag{5}$$

is the state vector, where m denotes the sample index according to a sample spacing of T_{GPS}.

Next, the true turn rates $\omega(k)$ and forward velocities $s(k)$ are generated at the gyroscope's sampling times $k{\cdot}T_{\text{Gyro}}$ [4].

For the computation of $\omega(k)$, the vehicle's heading

$$\alpha(k) = \arctan\left(\frac{v_y(k{\cdot}T_{\text{Gyro}})}{v_x(k{\cdot}T_{\text{Gyro}})}\right) \tag{6}$$

is calculated in a first step. Next, the turn rate is calculated by the heading changes between two successive gyroscope sampling times:

$$\omega(k) = \frac{\alpha(k+1) - \alpha(k)}{T_{\text{Gyro}}}. \tag{7}$$

To obtain the forward velocity, the length of a circle segment is calculated, which is defined by the angles $\alpha(k)$, $\alpha(k+1)$ and the Cartesian coordinates $(x(k{\cdot}T_{\text{Gyro}}), y(k{\cdot}T_{\text{Gyro}}))$ and $(x((k+1){\cdot}T_{\text{Gyro}}), y((k+1){\cdot}T_{\text{Gyro}}))$. Dividing this length by T_{Gyro} gives the forward velocity $s(k)$.

Finally, reference values $s''(l)$ for the GSM based velocity estimation are generated every $T_{\text{GSM}} = 5{\cdot}T_{\text{Gyro}}$ seconds as the average of the forward velocity values within this interval. Here, l is the discrete time index counting multiples of the sampling interval T_{GSM} of the GSM based velocity estimator.

Note that in our notation, the primes are meant to distinguish different sampling intervals of the same underlying stochastic process, e.g. $s(k)$ denotes the process s sampled at times $k{\cdot}T_{\text{Gyro}}$, $s'(m)$ corresponds to s sampled with a spacing T_{GPS}, and $s''(l)$ is s sampled with a sampling interval of T_{GSM}.

In the following subsection we describe how the the ground truth values are distorted to account for the imperfections of the different sensors.

B. Generation of GPS Position Measurements

Instantaneous GPS measurements

$$\boldsymbol{z}_{\text{GPS}}(m) = \begin{pmatrix} \tilde{x}(m{\cdot}T_{\text{GPS}}) \\ \tilde{y}(m{\cdot}T_{\text{GPS}}) \end{pmatrix} \tag{8}$$

of the location are generated using the following measurement equation:

$$\boldsymbol{z}_{\text{GPS}}(m) = \begin{pmatrix} 1 & 0 & 0 & 0 \\ 0 & 1 & 0 & 0 \end{pmatrix} \cdot \boldsymbol{x}'_{\text{True}}(m) + \boldsymbol{v}_{\text{GPS}}(m). \tag{9}$$

Here, $\boldsymbol{v}_{\text{GPS}}(m) \sim \mathcal{N}(0, 1800 \cdot \boldsymbol{I}_2)$ is white Gaussian measurement noise. Further details concerning the covariance matrix will be given later on.

We assume that the GPS receiver does not directly measure the velocity, which is a quite reasonable assumption for low cost GPS receivers.

C. Generation of Gyroscope Data

For the turn rate measurements $\tilde{\omega}(k)$ of the gyroscope, a gyroscope measurement model including drift [5] was implemented. The time-dependent drift $\epsilon(k)$ of the gyroscope, which results in a deviation of the measured turn rate from the true value is modelled as an exponential function

$$\epsilon(k) = C_1\left(1 - e^{-\frac{k{\cdot}T_{\text{Gyro}}}{T_{\text{Drift}}}}\right) + C_2, \tag{10}$$

with parameters C_1, C_2, and T_{Drift}.

The measurement model was furthermore extended to include noise, quantization errors of the measured turn rates and nonlinearity. Due to the lack of an appropriate model,

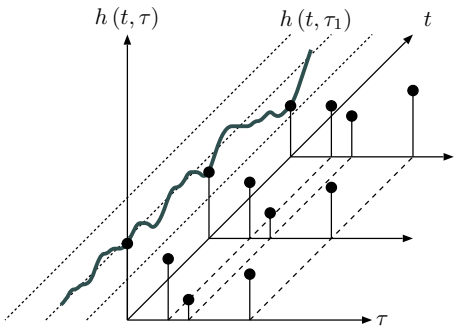

Fig. 2. Principle of fast fading estimation

the nonlinearity was modelled as an sine function of the true turn rate. Thus the overall measurement equation is given by:

$$\tilde{\omega}(k) = f(\omega(k)) + \epsilon(k) + v_{\text{Gyro}}(k). \tag{11}$$

Here, $f(\cdot)$ stands for the effects caused by quantization and nonlinearity. $v_{\text{Gyro}}(k) \sim \mathcal{N}\left(0, \sigma^2_{\text{Gyro}}\right)$ is the scalar measurement noise. All parameters are chosen such that a precision which is typical of existing low cost gyroscopes is reached [6], [7], [8]: The resolution of the gyroscope measurements was 0.1 degree per second, the nonlinearity was set to be four percent, and the variance of the measurement noise was $\sigma^2_{\text{Gyro}} = \frac{24}{100000}$.

D. Estimation of Forward Velocity from GSM Data

The true forward velocity is used in the generation of GSM downlink signals received by the mobile GSM unit, as it influences the fading statistics of GSM. The simulated downlink contains all relevant aspects of GSM signalling such as burst structures, differential encoding, Gaussian minimum shift keying (GMSK) pulse shaping, and a realistic channel. The implemented channel model accounts for additive white Gaussian noise, cochannel interference, and furthermore multipath propagation according to the bad urban profile of COST 207 [9].

For each path i of the multipath profile with corresponding delay τ_i an independent fast fading process $h(t,\tau_i)$ is defined, with t denoting the time-variance of the channel, see figure 2. Assuming a uniform distribution of the angle of arrival of the signal components (isotropic scattering), the power spectral density of this process exhibits the typical u-shaped form (so-called Jakes' spectrum), see figure 3:

$$S_i(f) = \begin{cases} \frac{\sigma_i^2}{\pi} \cdot \frac{f_{D_{\max}}}{\sqrt{f^2_{D_{\max}} - f^2}} & \text{for } |f| < f_{D_{\max}}, \\ 0 & \text{else.} \end{cases} \tag{12}$$

σ_i^2 is the average signal power of the i-th path and f denotes the frequency. The maximum Doppler frequency shift $f_{D_{\max}}$ depends on the forward velocity s, the carrier frequency f_C, and the radio wave propagation speed, which is usually the speed of light c:

$$f_{D_{\max}} = s \cdot \frac{f_C}{c}. \tag{13}$$

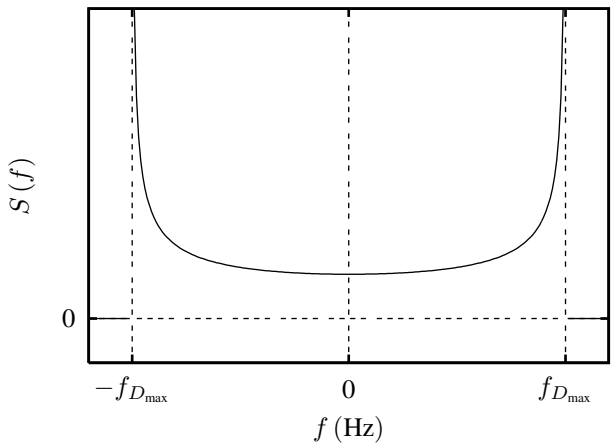

Fig. 3. Power spectral density of a fast fading process for isotropic scattering: Jakes' spectrum

The forward velocity is estimated in the GSM receiver in a 2-step process. First the channel impulse response $h(t,\tau)$ is estimated from training data which are periodically sent on the base station's pilot channel [10], [11]. Then the Doppler spectrum $\hat{S}_1(f)$ is estimated from the Fourier transform of the first multipath component's estimation $\hat{h}(t,\tau_1)$ w.r.t. the time variable t.

By assuming a power spectral density of the shape of equation (12) for the estimated fast fading process $\hat{h}(t,\tau_1)$, the forward velocity can finally be estimated by an approach called velocity estimation using the power spectral density (VEPSD) [12]. The main idea is that the highest slope in the power spectral density corresponds to the maximum Doppler frequency shift and thus to the current forward velocity. An estimate of the forward velocity is obtained by:

$$\tilde{s} = \frac{c}{f_C} \max\left\{ \underset{f}{\text{argmax}} \left\{ \left| \frac{d}{df} \hat{S}_1(f) \right| \right\} \right\}. \tag{14}$$

Here, the argmax operator has to be understood to return the location of one or more local maxima. The maximum operation then picks the largest frequency at which a local maximum occurs.

This estimation process does not require an active connection. The resulting estimates, however, suffer from delays and averaging caused by the temporal window required to compute the power spectral density. Furthermore it turned out that mean and variance of the estimation error depend on the true velocity. This can be modelled by the following measurement equation:

$$\tilde{s}''(l) = s''(l) + v_{\text{GSM}}(l, s''(l)), \tag{15}$$

with

$$v_{\text{GSM}}(l, s''(l)) \sim \mathcal{N}\left(\mu(s''(l)), \sigma^2(s''(l))\right) \tag{16}$$

being an approximation of the measurement noise modelling a Gaussian distributed measurement error.

Note that the period $T_{\text{GSM}} = \frac{120}{1625}$ [s], at which the GSM based velocity estimates occur, is defined on the basis of the timing used for GSM signalling and on basis of the temporal window length required to compute the power spectral density. The gyroscope's sampling time is set to $T_{\text{Gyro}} = \frac{T_{\text{GSM}}}{5}$ in order to keep the dead reckoning, which is performed later, as simple as possible. The resulting gyroscope's sampling frequency of $\frac{1}{T_{\text{Gyro}}} = 67.71$ Hertz lies within the range of typical low cost gyroscopes.

III. Sensor Fusion Architecture

Figure 4 depicts the architecture of our proposed positioning system. At first, all measurement data are passed through individual (extended) Kalman filters in order to get higher precision data for the sensor fusion. In a second step, dead reckoning is performed employing the gyroscope data and the GSM based speed estimates. Filtered GPS data are utilized to correct the computed position estimates.

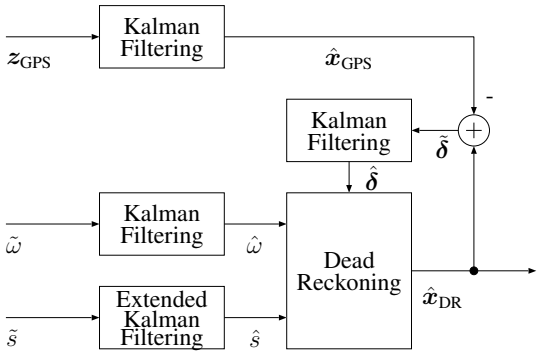

Fig. 4. Architecture of the Positioning System

A. Processing of instantaneous GPS position estimates

The instantaneous GPS measurements $\boldsymbol{z}_{\text{GPS}}$ are first input to a Kalman filter (KF) which yields at its output estimates

$$\hat{\boldsymbol{x}}_{\text{GPS}}(m) = \begin{pmatrix} \hat{x}(m{\cdot}T_{\text{GPS}}) \\ \hat{y}(m{\cdot}T_{\text{GPS}}) \\ \hat{v}_x(m{\cdot}T_{\text{GPS}}) \\ \hat{v}_y(m{\cdot}T_{\text{GPS}}) \end{pmatrix} \tag{17}$$

of location and velocity every T_{GPS} seconds. This filter is based on a state equation analogous to (2), however with sampling time T_{GPS}, and the measurement equation (9).

The covariance matrices for both system and measurement noise are assumed unknown and are estimated by separate training data. In practice, these training data can be acquired by using a reference high precision positioning system. The filter is initialized by two point differencing [3]: The first two instantaneous measurements are employed to initialize the estimated state vector and the corresponding covariance matrix of the filter's estimation error. Thus, no a priori knowledge about the system state is required.

Note that the covariance matrix of the measurement noise, see equation (9), has been chosen such that the Kalman filtered estimates exhibit accuracies with a root mean square (RMS) error of about 25 [m], which is typical of current low cost receivers [13].

B. Processing of Gyroscope Data

For the gyroscope data, a Kalman filter is applied in order to reduce the measurement error and to eliminate the deterministic drift in one step. To this end, the state vector of the Kalman filter is augmented by the derivatives $\dot{\omega}$, $\ddot{\omega}$ of the turn rate and by the drift ϵ and its derivative $\dot{\epsilon}$:

$$\boldsymbol{x}_{\text{Gyro}}(k) = \begin{pmatrix} \omega(k) \\ \dot{\omega}(k) \\ \ddot{\omega}(k) \\ \epsilon(k) \\ \dot{\epsilon}(k) \end{pmatrix}. \tag{18}$$

From equation (10) we find $\dot{\epsilon}(k) = \frac{C_1}{T_{\text{Drift}}} \cdot e^{-\frac{k \cdot T_{\text{Gyro}}}{T_{\text{Drift}}}}$, which can be utilized for the following recursive description of the drift:

$$\dot{\epsilon}(k+1) = e^{-\frac{T_{\text{Gyro}}}{T_{\text{Drift}}}} \cdot \dot{\epsilon}(k), \tag{19}$$

$$\epsilon(k+1) = \epsilon(k) + T_{\text{Drift}} \left(1 - e^{-\frac{T_{\text{Gyro}}}{T_{\text{Drift}}}}\right) \dot{\epsilon}(k). \tag{20}$$

These equations can be gathered in the state equation

$$\boldsymbol{x}_{\text{Gyro}}(k+1) = \boldsymbol{A}_{\text{Gyro}} \boldsymbol{x}_{\text{Gyro}}(k) + \boldsymbol{B}_{\text{Gyro}} \cdot w_{\text{Gyro}}(k), \tag{21}$$

with the state transition matrix

$$\boldsymbol{A}_{\text{Gyro}} = \begin{pmatrix} 1 & T_{\text{Gyro}} & \frac{T_{\text{Gyro}}^2}{2} & 0 & 0 \\ 0 & 1 & T_{\text{Gyro}} & 0 & 0 \\ 0 & 0 & 1 & 0 & 0 \\ 0 & 0 & 0 & 1 & T_{\text{Drift}} \cdot \left(1 - e^{-\frac{T_{\text{Gyro}}}{T_{\text{Drift}}}}\right) \\ 0 & 0 & 0 & 0 & e^{-\frac{T_{\text{Gyro}}}{T_{\text{Drift}}}} \end{pmatrix}. \tag{22}$$

By comparison with equations (10) and (19) we find the initialization: $\epsilon(0) = C_2$, $\dot{\epsilon}(0) = \frac{C_1}{T_{\text{Drift}}}$.

The matrix $\boldsymbol{B}_{\text{Gyro}}$ which relates the scalar white, Gaussian system noise $w_{\text{Gyro}}(k)$ to the system state is given by

$$\boldsymbol{B}_{\text{Gyro}} = \begin{pmatrix} \frac{T_{\text{Gyro}}^2}{2} \\ T_{\text{Gyro}} \\ 1 \\ 0 \\ 0 \end{pmatrix}. \tag{23}$$

The equation (11) is simplified to the measurement equation

$$\tilde{\omega}(k) = \begin{pmatrix} 1 & 0 & 0 & 1 & 0 \end{pmatrix} \cdot \boldsymbol{x}_{\text{Gyro}}(k) + \tilde{v}_{\text{Gyro}}(k), \tag{24}$$

with a white Gaussian measurement noise $\tilde{v}_{\text{Gyro}}(k)$.

Note that $\tilde{v}_{\text{Gyro}}(k)$ has an increased variance compared to $v_{\text{Gyro}}(k)$ as it also captures the effects of the quantization errors.

Again, the statistical properties of both system and measurement noise are estimated by separate training data. Also, the gyroscope parameters C_1, C_2, and T are estimated from

training data using the Levenberg-Marquardt method of iterative least squares. The filter is again initialized by two point differencing.

By applying this kind of filtering, the estimate $\hat{\boldsymbol{x}}_{\text{Gyro}}(k)$ is computed, of which $\hat{\omega}(k) = \begin{pmatrix}1 & 0 & 0 & 0 & 0\end{pmatrix} \cdot \hat{\boldsymbol{x}}_{\text{Gyro}}(k)$ is utilized in the dead reckoning step performed later on.

C. Processing of GSM based Velocity Estimates

Another state estimator is applied to the forward velocity 'measurements' $\tilde{s}''(l)$ computed from the analysis of the GSM fading statistics. The following state equation is used:

$$x_{\text{GSM}}(l+1) = x_{\text{GSM}}(l) + B_{\text{GSM}} \cdot w_{\text{GSM}}(l), \tag{25}$$

with state variable

$$x_{\text{GSM}}(l) = s''(l). \tag{26}$$

B_{GSM} is given by $B_{\text{GSM}} = T_{\text{GSM}}$, if a random white acceleration is assumed.

The measurement equation (15) is nonlinear due to the dependence of the statistics of the measurement noise $v_{\text{GSM}}(l, s''(l))$ on the velocity $s''(l)$. Therefore, extended Kalman filtering (EKF) has to be used. This nonlinear dependency is modelled by a polynomial function of order 4, thus

$$v_{\text{GSM}}(l, s''(l)) \sim \mathcal{N}\left(\sum_{i=0}^{4} a_i \cdot (s''(l))^i, \sum_{i=0}^{4} b_i \cdot (s''(l))^i\right), \tag{27}$$

with coefficients also being trained on separate training data by regression. The variance of the system noise w_{GSM} is again estimated on separate training data, and the filter is initialized by two point differencing.

D. Dead Reckoning and Sensor Fusion

Using the more reliable filtered estimates $\hat{\omega}(k)$ and $\hat{s}''(l)$, corresponding values

$$\hat{\boldsymbol{x}}_{\text{DR}}(k) = \begin{pmatrix} \hat{x}_{\text{DR}}(k \cdot T_{\text{Gyro}}) \\ \hat{y}_{\text{DR}}(k \cdot T_{\text{Gyro}}) \\ \hat{v}_{x,\text{DR}}(k \cdot T_{\text{Gyro}}) \\ \hat{v}_{y,\text{DR}}(k \cdot T_{\text{Gyro}}) \end{pmatrix} \tag{28}$$

for position and speed are calculated every T_{Gyro} seconds in a recursive manner by computing offset vectors (core principle of dead reckoning). However, the error

$$\boldsymbol{\delta}_{\text{True}}(k) = \hat{\boldsymbol{x}}_{\text{DR}}(k) - \boldsymbol{x}_{\text{True}}(k) \tag{29}$$

concerning the position calculated by this approach increases over time due to the recursive computation.

To combat this effect, an error model according to the architecture presented in [14] is defined, by which an error estimate $\hat{\tilde{\boldsymbol{\delta}}}(m)$ is used for correction of the estimated position and velocity. Here, $\hat{\tilde{\boldsymbol{\delta}}}(m)$ is estimated from the difference $\tilde{\boldsymbol{\delta}}(m)$ of the position estimates obtained by GPS and dead reckoning:

$$\tilde{\boldsymbol{\delta}}(m) = \hat{\boldsymbol{x}}'_{\text{DR}}(m) - \hat{\boldsymbol{x}}_{\text{GPS}}(m). \tag{30}$$

Note that the index m indicates that this error estimate can only be calculated at the sampling times $m \cdot T_{\text{GPS}}$ of the GPS receiver.

The error estimate $\tilde{\boldsymbol{\delta}}(m)$ is input to a Kalman filter. Again, a system model analogous to equation (2) is employed:

$$\boldsymbol{\delta}'_{\text{True}}(m+1) = \boldsymbol{A}_{\text{Error}} \boldsymbol{\delta}'_{\text{True}}(m) + \boldsymbol{B}_{\text{Error}} \boldsymbol{w}_{\text{Error}}(m), \tag{31}$$

however now with the error $\boldsymbol{\delta}'_{\text{True}}(m)$ sampled at times $m \cdot T_{\text{GPS}}$ being the state variable. $\boldsymbol{A}_{\text{Error}}$ and $\boldsymbol{B}_{\text{Error}}$ correspond to the variables utilized in the Kalman filter for the instantaneous GPS estimates. Again, $\boldsymbol{w}_{\text{Error}}(m)$ is white Gaussian system noise corresponding to a random acceleration.

With equations (29) and (30) the measurement equation can be written as follows:

$$\begin{aligned} \tilde{\boldsymbol{\delta}}(m) &= \boldsymbol{\delta}'_{\text{True}}(m) + (\boldsymbol{x}'_{\text{True}}(m) - \hat{\boldsymbol{x}}_{\text{GPS}}(m)), & (32) \\ &= \boldsymbol{\delta}'_{\text{True}}(m) + \boldsymbol{v}_{\text{Error}}(m), & (33) \end{aligned}$$

with $\boldsymbol{v}_{\text{Error}}(m) \sim \mathcal{N}\left(\boldsymbol{\mu}_{\text{Error}}, \boldsymbol{\sigma}^2_{\text{Error}}\right)$ being Gaussian measurement noise defined by the the statistical properties of the estimation error of the GPS Kalman filter.

Whenever there is a GPS measurement available, a new estimate of the error is calculated by which the position and heading of the dead reckoning is corrected.

Due to the recursive structure of this sensor fusion problem (the Kalman filtered error estimate $\hat{\tilde{\boldsymbol{\delta}}}(m)$ affects and is affected by $\hat{\boldsymbol{x}}'_{\text{DR}}(m)$), the statistics of the system and measurement noise have to be estimated in an iterative manner. At first, the GPS estimates are replaced by the ground truth values and no error filtering is performed in order to compute a first estimation of the system noise of the error filter. In the following iterations, Kalman filtering using the estimated system noise is performed and the system and measurement noise are reestimated.

IV. Experimental Results

We conducted experiments on a synthetical trajectory of a length of 31 [km]. The virtual drive on that trajectory took approximately 22 minutes.

A. Pure Dead Reckoning

At first, the performance of pure dead reckoning is evaluated. Figure 5 depicts the mentioned trajectory (bold line) and two estimates calculated by different approaches. The grey dotted line results from dead reckoning with unfiltered gyroscope measurements and GSM based velocity estimates, whereas the black dotted curve was estimated by using corresponding filtered data. Both approaches did not employ GPS data for correction. It can be seen, that using unfiltered data delivers completely unreliable estimates. Utilizing filtered measurement data, dead reckoning is able to track the trajectory at the beginning. But quickly the positioning error increases, rendering this approach unsuitable, even though the shape of the resulting trajectory has a certain similarity with the reference trajectory. This growing error is the reason why dead reckoning only makes sense in conjunction with correcting data from another sensor device.

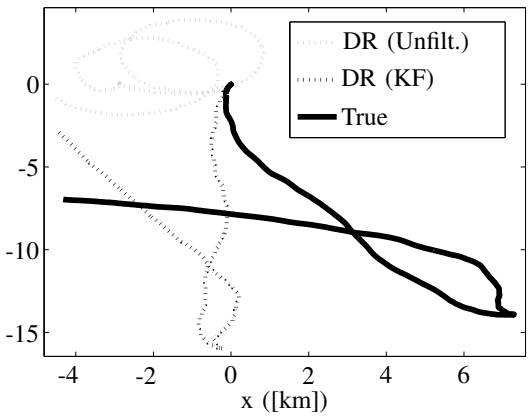

Fig. 5. Trajectories estimated by pure dead reckoning

B. Sensor Fusion in Comparison to pure GPS Positioning

Figure 6 contains plots of the cumulative density functions (CDFs). For a given distance, the CDF gives the probability that the obtained absolute positioning error is smaller than or equal to that distance. A perfect localization method would have a constant cumulative density function of 1 for every distance since its error would always be 0 [m]. It can be clearly seen that the instantaneous GPS estimates, plotted as a grey dashed line, can be improved by Kalman filtering whose results are given by the solid grey line. Better positioning performance can be obtained by our hybrid positioning system employing GSM based velocity estimates and gyroscope data (solid black line): While for 67 percent of all cases the positioning error is smaller than or equal to 26.19 [m] for pure Kalman filtered GPS estimates, it is below or equal 22.61 [m] for the proposed positioning system.

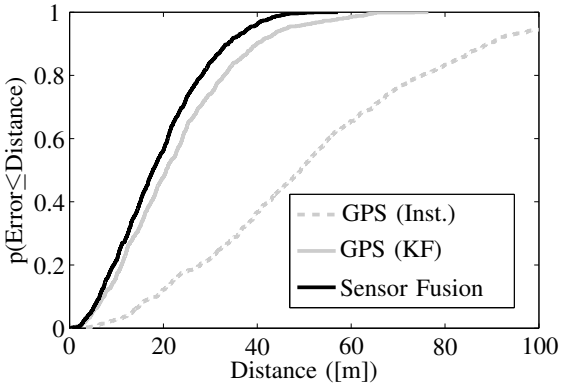

Fig. 6. Cumulative density function of the positioning errors

Table I shows some additional performance indicators of the obtained positioning errors: the RMS error, the mean absolute error, the maximum absolute error, and the variance of the absolute error. It can be seen clearly, that the sensor fusion approach performs best w.r.t. every indicator.

Approach:	RMS Error:	Mean abs. Error:	Max. abs. Error:	Error Variance:
GPS	26.20 [m]	22.63 [m]	76.46 [m]	174.29 [m^2]
Sensor Fusion	21.76 [m]	19.11 [m]	57.18 [m]	108.32 [m^2]

TABLE I
ERROR PROPERTIES OF LOCALIZATION

C. Sensor Fusion in Comparison to pure GPS Positioning for degraded GPS Signal Quality

In a next step we conducted experiments concerning a disturbed GPS reception. In order to model a distorted GPS channel, the Gilbert-Elliot model is employed, which is a two state model, the one state indicating availability of GPS and the other absence of GPS. In the figure 7, 'R' (Reception) denotes the state where the GPS signal is received, while L stands for loss of the GPS signal. The transition probabilities $(1-q)$ and $(1-p)$ between these states determine the severeness of the degradation, where the probability of loosing the GPS signal is given by $(1-p)$ and the burstiness of the distortion is given by q, the probability of remaining in state 'L'.

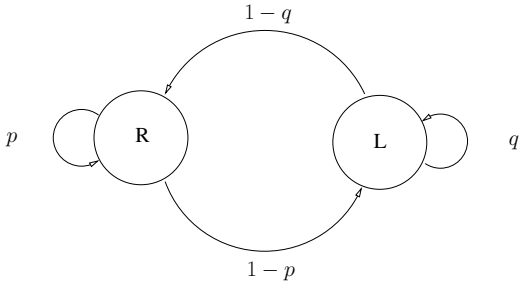

Fig. 7. Gilbert-Elliot channel model

Both probabilities have been estimated by analyzing long term statistics of a low cost GPS receiver placed in our laboratory one meter away from the window. This position inside the building has a degraded visibility of GPS satellites and was meant to be comparable to GPS receiving conditions in narrow street canyons. The obtained probabilities are $p = 0.99$ and $q = 0.82$. In order to model an even more unreliable GPS channel, we used the probabilities $p' = \frac{p}{1.1}$ and $q' = 1.1 \cdot q$. By this, for 43 percent of all GPS sampling times no position information is available.

The CDF plots depicted in figure 8 visualize the obtained results. In comparison to figure 6, a decreased performance can be seen, which is not surprising due to the degraded GPS reception. In 67 percent of all estimates the GPS positioning error is now equal to or smaller than 45.68 [m], whereas the error is smaller than or equal to 31.94 [m] with the sensor fusion approach.

The corresponding performance indicators of the obtained errors are outlined in table II. Again, the hybrid approach performs best. We conclude that our approach is able to enhance the robustness of positioning.

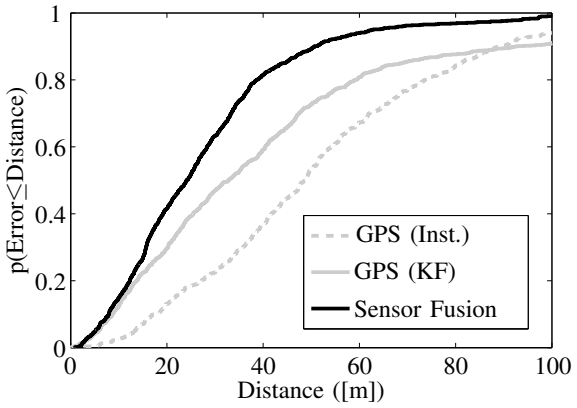

Fig. 8. Cumulative density function of the positioning errors for a degraded GPS channel

Approach:	RMS Error:	Mean abs. Error:	Max. abs. Error:	Error Variance:
GPS	60.17 [m]	43.65 [m]	263.55 [m]	1715.24 [m^2]
Sensor Fusion	34.03 [m]	27.77 [m]	115.63 [m]	386.86 [m^2]

TABLE II
ERROR PROPERTIES OF LOCALIZATION FOR A DEGRADED GPS CHANNEL

In the following, we illustrate the effect of the loss of the GPS signal by means of an example. Figure 9 contains a part of the trajectory where a drop out of the GPS signal occurred. Again, the bold black line is the true trajectory. The grey dots depict instantaneous GPS measurements and the section of the trajectory where there is no GPS signal available can be seen clearly. The grey line shows the results obtained by Kalman filtering the GPS measurements. As the Kalman filter can only predict the position during the absence of the GPS signal, its positioning error increases over time. The prediction results in the straight line seen in the figure. As soon as GPS is available again, the Kalman filter recovers. The thin black line corresponds to the trajectory estimation calculated by our sensor fusion system. During the drop out of GPS, this system is still able to follow the true trajectory quite well by performing dead reckoning on the filtered gyroscope turn rates and GSM based velocity estimates.

In Figure 10, the positioning error of a larger part of the reference trajectory is plotted over time. It can be clearly seen that the error of our hybrid positioning system (black line) increases only mildly during drop out, while it rises quickly in the case of GPS-only positioning (grey line).

D. Comparison of GSM based Velocity Estimates with Odometer Data

Finally we investigated the impact of the GSM based velocity estimates on the positioning performance as compared to speed information obtained from the vehicle's CAN interface. A car's odometer must comply to European regulations [15]: the speed estimate is not allowed to be lower than the true value and must not exceed the true value by more than 10 percent plus 4 [$\frac{km}{h}$]. We conducted experiments simulating a

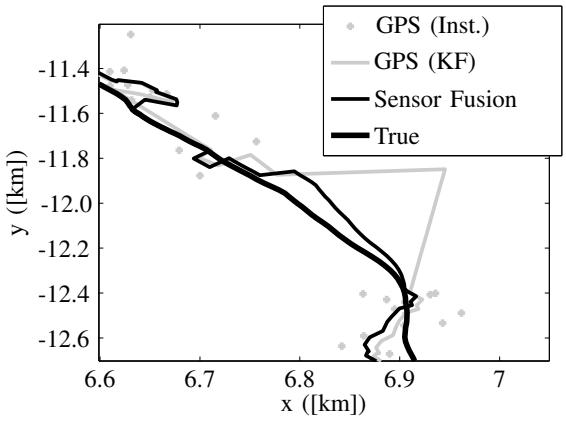

Fig. 9. Sample trajectory with a GPS signal drop out

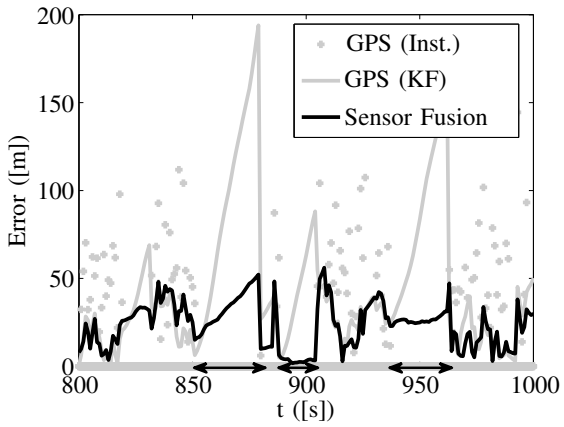

Fig. 10. Positioning error over time in the case of GPS signal drop outs (time periods of signal drop outs marked)

perfect odometer and an odometer with a maximum tolerable error, both for perfect GPS reception. The obtained results are depicted in figure 11.

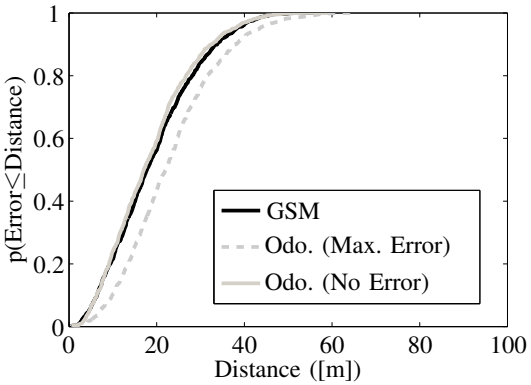

Fig. 11. Cumulative density function of the positioning errors for tachometers with different precision

Compared to an ideal odometer (solid grey line), our approach (black line) performs quite well. If the perfect odometer is used in the sensor fusion, in 67 percent of all estimations

the positioning error is smaller than or equal to 21.88 [m]. The dashed grey line corresponds to the results obtained by an odometer with a maximum allowable error. Here a positioning error of 26.77 [m] or less is achieved in 67 percent.

The corresponding performance indicators of the obtained errors are shown in table III. Comparing these results to those obtained by GSM based velocity estimation, see table I, we can state that GSM based velocity estimates are indeed a competitive alternative to the car's odometer measurements.

Approach:	RMS Error:	Mean abs. Error:	Max. abs. Error:	Error Variance:
Odometer, no Error	21.03 [m]	18.45 [m]	17.10 [m]	101.91 [m^2]
Odometer, max. Error	25.64 [m]	23.13 [m]	64.00 [m]	122.39 [m^2]

TABLE III
ERROR PROPERTIES OF LOCALIZATION UTILIZING TACHOMETER DATA OF DIFFERENT PRECISION

V. CONCLUSIONS

In this paper we have proposed a positioning system for supporting GPS localization with GSM based velocity estimates and gyroscope turn rate measurements. No active connection is required to compute GSM based speed estimates, thus no service charges will emerge from such an approach.

Experimental results show that positioning using this approach is more accurate and more robust compared to GPS-only positioning. We also replaced the GSM based velocity estimates with perfect odometer data and it turned out that our approach delivers positioning estimates of only slightly degraded quality. Thus, the velocity estimates obtained by GSM seem to be a viable alternative to odometer readings which require access for the vehicle's CAN bus.

However, so far we assumed perfect time and frequency synchronization in the GSM receiver. These imperfections need to be taken into account in future work.

We will also focus on an analytical description of the measurement noise of the GSM based velocity estimations in order to obtain even more accurate speed information.

REFERENCES

[1] Peschke, S. and Haeb-Umbach, R., "Velocity Estimation of Mobile Terminals by Exploiting GSM Downlink Signalling", *Proceedings of the 4th Workshop on Positioning, Navigation, and Communication 2007*, Hanover, Germany, March 2007

[2] Haeb-Umbach, R. and Peschke, S., "Particle Filtering of Database assisted Positioning Estimates using a novel Similarity Measure for GSM Signal Power Level Measurements", *Proceedings of the 3rd Workshop on Positioning, Navigation, and Communication 2006*, Hanover, Germany, March 2006

[3] Bar-Shalom, Y., Rong Li, X., and Kirubarajan, T., *Estimation with Applications to Tracking and Navigation*, New York, NY, USA, John Wiley & Sons Inc., 2001

[4] Obdradovic, D., Lenz, H., and Schupfner, M., "Fusion of Sensor Data in Siemens Car Navigation System", *IEEE Transactions on Vehicular Technology*, vol. 56, no. 1, pp. 43-49, January 2007

[5] Barshan, B. and Durrant-Whyte, H.F., "Inertial Navigation Systems for Mobile Robots", *IEEE Transactions on Robotics and Automation*, vol. 11, no. 3, pp. 328-342, June 1995

[6] Bosch, *Yaw Rate Sensor YRS 2*, Bosch, May 2006

[7] Panasonic, *Angular Rate Sensors/EWTS82*, Panasonic, March 2005

[8] Panziere, S., Pascucci, F., and Ulivi, G., "An Outdoor Navigation System Using GPS and Inertial Platform", *IEEE/ASME Transactions on Mechatronics*, vol. 7, no. 2, June 2002

[9] European Commission, "Digital land mobile radio communications", *COST 207 Final Report*, CEC Publications, EUR 12160 EN, 1989

[10] European Telecommunication Standards Institute, *European digital cellular telecommunications system (Phase 2): Physical layer on the radio path, General description (ETS 300 573: July 1995 (GSM 05.01 version 4.4.0))*, Sophia Antipolis, France, ETSI, July 1995

[11] European Telecommunication Standards Institute, *Recommendation GSM 05.02, Radio Sub-system Link Control (Version 3.8.0)*, Sophia Antipolis, France, ETSI, December 1995

[12] Mohanty, S., "VEPSD: A Novel Velocity Estimation Algorithm for Next-Generation Wireless Systems", *IEEE Transactions on Wireless Communications*, vol. 4, no. 6, pp. 2655-2660, November 2005

[13] Modsching, M., Kramer, R., and ten Hagen, K., "Field trial on GPS Accuracy in a medium size city: The influence of built up", *Proceedings of the 3rd Workshop on Positioning, Navigation, and Communication 2007*, Hanover, Germany, March 2006

[14] Cramer, M., *Genauigkeitsuntersuchungen zur GPS/INS-Integration in der Aerophotogrammetrie*, Ph.D. thesis, Stuttgart, Germany, 2001

[15] United Nations Economic Commission for Europe, Transport Division, *Vehicle Regulations: Addendum 38, Regulation 39*, United Nations, February 2003